



## RESEARCH LETTER

10.1002/2013GL059153

## Key Points:

- Outflow of Antarctic dense shelf water through troughs generates TVWs
- Wave frequency depends on the amount of stretching induced in ambient fluid
- TVW energy flux is generally eastward, opposing phase propagation

## Supporting Information:

- Readme
- Text S1
- Movie S1

## Correspondence to:

G. M. Marques,  
gmarques@rsmas.miami.edu

## Citation:

Marques, G. M., L. Padman, S. R. Springer, S. L. Howard, and T. M. Özgökmen (2014), Topographic vorticity waves forced by Antarctic dense shelf water outflows, *Geophys. Res. Lett.*, *41*, 1247–1254, doi:10.1002/2013GL059153.

Received 26 DEC 2013

Accepted 29 JAN 2014

Accepted article online 4 FEB 2014

Published online 22 FEB 2014

## Topographic vorticity waves forced by Antarctic dense shelf water outflows

Gustavo M. Marques<sup>1</sup>, Laurie Padman<sup>2</sup>, Scott R. Springer<sup>3</sup>, Susan L. Howard<sup>3</sup>, and Tamay M. Özgökmen<sup>1</sup>

<sup>1</sup>Division of Meteorology and Physical Oceanography, Rosenstiel School of Marine and Atmospheric Science, University of Miami, Miami, Florida, USA, <sup>2</sup>Earth & Space Research, Corvallis, Oregon, USA, <sup>3</sup>Earth & Space Research, Seattle, Washington, USA

**Abstract** We use numerical simulations to investigate excitation of topographic vorticity waves (TVWs) along the Antarctic continental slope by outflows of dense shelf water through troughs. Idealized models show that wave frequency depends on the amount of stretching in the ambient fluid over the outflow and on background along-slope mean flow. Frequency is higher for steeper bottom slope, larger outflow density anomaly, and stronger westward mean flow. For weak stratification and weak westward along-slope flows typical of the Antarctic slope, wave energy propagates eastward, in the opposite direction from phase velocity. Our results are consistent with recent observations of TVWs in the southern Weddell Sea. In a realistic simulation of the Ross Sea, TVW properties are modulated on seasonal and shorter time scales as background ocean state varies. We expect these waves to affect mixing, cross-slope exchanges, and sea ice concentration in the vicinity of sources of dense water outflows.

## 1. Introduction

Antarctic Bottom Water (AABW) is produced along the Antarctic continental margins where cold, dense shelf water (DSW) flows off the continental shelf and mixes with ambient water masses including Circumpolar Deep Water. The production rate and hydrographic characteristics of the resulting AABW depend on small-scale advection and mixing processes along the outer continental shelf and slope [e.g., Gill, 1973; Orsi, 1999].

Numerical simulations [Wang *et al.*, 2009] and observations [Jensen *et al.*, 2013] show subinertial, quasi-periodic oscillations in water properties along the upper continental slope in the southern Weddell Sea. These oscillations, whose properties are consistent with mode-1 coastal-trapped waves [Jensen *et al.*, 2013], can be sufficiently energetic (currents of  $\sim 0.1\text{--}0.4\text{ m s}^{-1}$ ) to make a significant contribution to total mixing along the slope through added benthic stress at the seabed. Therefore, we expect that these waves will affect the exchange of water mass properties between the deep Southern Ocean and Antarctica's shelf seas and should therefore be represented in coupled climate models.

We refer to these waves as topographic vorticity waves (TVWs) [Platzman *et al.*, 1981], since they depend on the large bathymetry gradient across the continental slope rather than distance from the coast. Jensen *et al.* [2013] hypothesized that the TVWs they observed in the southern Weddell Sea were generated by release of DSW from Filchner Trough but did not confirm it. Periodicity in dense outflows has previously been observed in laboratory studies [e.g., Lane-Serff and Baines, 1998], providing an oscillatory forcing for TVWs that can subsequently propagate along the continental slope. At the typical periods of these waves, 1–2 days [Jensen *et al.*, 2013], dispersion curves for weak stratification typical of Antarctic seas have two solutions, with potential for energy propagation in both directions from the source. Propagation of TVWs to the west of the source, i.e., in the same direction as the dense water outflow, will affect mixing of the outflow and the volume flux and hydrographic properties of the resulting AABW. Eastward propagation of TVWs will provide an energy source for mixing of water that is approaching the trough in the westward flowing Antarctic Slope Current (ASC) and so modify the properties of the water masses with which the DSW interacts as it exits the trough.

Here we use numerical models to investigate the generation of TVWs by Antarctic DSW outflows and the dependence of their dispersion properties on bottom slope, outflow density anomaly, and background

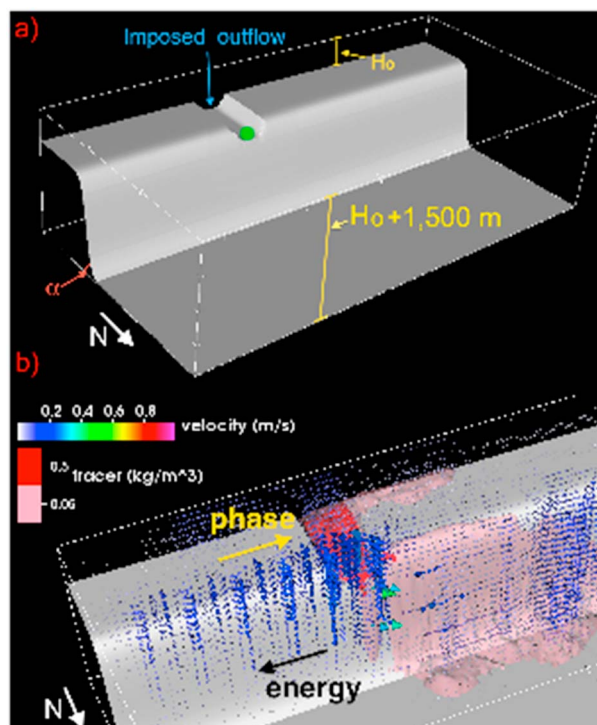


**Figure 1.** (a) Three-dimensional view of the domain for the idealized model. Green point shows the location where  $\Gamma$  values are computed. Thick marks are placed every 100 km in the horizontal and 500 m in the vertical directions. (b) Partial view of the idealized domain for the control experiment (see Table 1 Experiment number 01) at model time  $t = 78$  days, showing wave-like velocity structures east of the trough. The phase and energy directions and two contours of tracer concentration (0.5 and 0.05) are also shown. Corresponding animation can be found in the supporting information (Movie S1).

along-slope flow representing the ASC. This work is a first step toward developing ways to represent the effects of TVWs in climate models, whose coarse grids preclude explicit modeling of TVW generation and propagation.

## 2. Numerical Simulations

We use an idealized model of density outflows and a realistic, atmospherically forced model of the Ross Sea. Both models are based on the Regional Ocean Modeling System (ROMS) [Shchepetkin and McWilliams, 2005]. ROMS has been widely used, including applications to overflow-related studies [e.g., Ilicak et al., 2008; Padman et al., 2009].

### 2.1. Idealized Model of TVW Generation by Outflows

The model domain ( $600 \times 300$  km) is a flat continental shelf with depth  $H_0$ , a continental slope  $\alpha$ , and a flat abyssal ocean that is  $H_0 + 1500$  m deep (Figure 1a). The slope is located at latitude  $72^\circ\text{S}$ , corresponding to the Drygalski Trough outflow in the northwest Ross Sea [Padman et al., 2009; Gordon et al., 2009]. A half-cosine-shaped canyon, whose axis is centered  $\sim 200$  km from the eastern wall, cuts across the shelf with a maximum depth of  $H_0 + 200$  m and width of  $\sim 50$  km. The horizontal grid spacing ( $\Delta x$ ) is set to either 3 km or 1 km (see Table 1), with the finer spacing needed to resolve the slope when  $\alpha = 0.1$ . In the vertical direction, all experiments were discretized using 41 topography-following levels. Further details on the model configuration can be found in the supporting information (Text S1).

We carried out a set of 14 simulations (Table 1), varying  $\alpha$ ,  $H_0$ ,  $\Delta\rho$ ,  $\Delta x$ , and maximum along-slope barotropic velocity ( $U_{\max}$ , representing the ASC) over ranges representing typical observed values in the Weddell and Ross seas [Jacobs, 1991; Heywood et al., 1998; Foldvik et al., 2004; Muench et al., 2009]. In our control run (Experiment number 01), the main parameters were set as follows:  $\Delta x = 3$  km,  $\alpha = 0.05$ ,  $H_0 = 500$  m,  $U_{\max} = 0$  m s<sup>-1</sup>, and  $\Delta\rho = 0.24$  kg m<sup>-3</sup>. Boundary conditions were similar to those used in previous idealized simulations of overflows [Legg et al., 2006; Ilicak et al., 2011]. Most simulations were started from rest, except

**Table 1.** List of Numerical Experiments Conducted<sup>a</sup>

Exp. No.	$\Delta x$ (km)	$\alpha$	$H_0$ (m)	$\Delta\rho$ (kg m <sup>-3</sup> )	$U_{\max}$ (m s <sup>-1</sup> )	$\Gamma_{\min}$	$\Gamma_{\max}$	$\Gamma_{\text{av}}$	$\omega$ (cpd)	$\lambda$ (km)	$c_p$ (m s <sup>-1</sup> )	$c_g$ (m s <sup>-1</sup> )
01	3	0.05	500	0.24	0	0.19	0.41	0.33	0.48	39	-0.22	0.13
02	3	0.05	500	0.12	0	0.11	0.28	0.23	0.41	33	-0.16	0.10
03	1	0.05	500	0.24	0	0.09	0.35	0.22	0.52	42	-0.25	0.14
04	1	0.10	500	0.24	0	0.66	0.87	0.77	0.65	32	-0.24	0.11
05	3	0.01	500	0.24	0	0.11	0.11	0.11	0.15	60	-0.10	0.06
06	3	0.05	250	0.24	0	0.38	0.81	0.62	0.58	33	-0.22	0.03
07	3	0.05	750	0.24	0	0.14	0.28	0.22	0.45	45	-0.24	0.12
08	3	0.05	500	0.18	0	0.23	0.39	0.31	0.48	36	-0.20	0.12
09	3	0.01	750	0.12	0	0.03	0.03	0.03	0.10	48	-0.06	0.04
10	3	0.05	750	0.12	0	0.04	0.19	0.14	0.39	36	-0.16	0.10
11	1	0.10	250	0.12	0	0.39	1.10	0.72	0.83	29	-0.28	0.12
12	3	0.05	500	0.24	-0.1	0.09	0.32	0.20	0.55	42	-0.27	0.06
13	3	0.05	500	0.24	-0.2	0.15	0.18	0.18	0.71	54	-0.44	0.03
14	3	0.05	500	0.24	-0.3	0.17	0.17	0.17	0.77	57	-0.51	-0.03

<sup>a</sup>Values of  $c_p < 0$  and  $c_g < 0$  indicate westward along-slope phase and energy propagation, respectively.

those in which  $U_{\max} \neq 0$ . In the latter, the initial conditions (sea surface elevation and along-slope velocity) were set in geostrophic balance such that  $U_{\max}$  occurred at the shelf break and exponentially decayed within 10 km to the north and south. The ambient water in all runs was initially homogeneous, with temperature and salinity values set to 0.95°C and 32.5, respectively. Dense water was injected in the trough at the southern wall. A passive tracer with initial concentration  $\tau = 1$  was injected with the dense water and then used to track the bottom plume.

Since angular momentum is conserved, the stretching of overlying ambient water carried by the overflow is an important parameter controlling oscillations in the system. Following Lane-Serff and Baines [1998], we evaluated the stretching parameter  $\Gamma = R_d\alpha/D$ , where  $R_d = \sqrt{\Delta b_0 h_0}/f$  is the baroclinic radius of deformation (defined as in Legg *et al.* [2006]),  $D$  is the depth of the ambient fluid above the bottom density current,  $\Delta b_0$  is the buoyancy anomaly,  $h_0$  is the thickness of the bottom density current, and  $f$  is the Coriolis parameter. We estimated time-varying values of  $\Gamma(t)$ , between model time  $t = 70$  and 100 days, for a point at the northern end of the trough (for location, see Figure 1a). We computed  $\Gamma(t)$  every 2 h and then removed the lowest and highest 10% of the values, so that the cited range of  $\Gamma$  includes 80% of the data during the 30 day analysis period. For our control run,  $\Gamma(t)$  varied between 0.19 and 0.41, with a time-averaged value ( $\Gamma_{\text{av}}$ ) of 0.33. For the other experiments,  $\Gamma_{\text{av}}$  values ranged from 0.03 to 0.77 (see Table 1). Variations in  $\Gamma$  are controlled by both  $\Delta\rho$  and  $D$  (see supporting information for further details).

The wave properties in our simulations were estimated from time series of depth-averaged across-slope velocity extracted along a portion of the upper slope represented by the ( $H_0 + 400$ ) m isobath. Frequencies and wavelengths were estimated using a Fourier transform and correlation, respectively. We compared these wave properties with dispersion curves of inviscid coastal-trapped waves, obtained numerically by resonance iteration using the 2-D (depth versus across-slope direction) code developed by Brink [2006] (see supporting information for further details). This code allows specification of  $U_{\max}$ ; therefore, we computed separate dispersion curves for experiment numbers 12–14.

## 2.2. Realistic Model of the Ross Sea

We used a ROMS model developed for realistic simulations of the Ross Sea [Dinniman *et al.*, 2011]. The horizontal grid spacing was 5 km, and the vertical grid consisted of 24 levels over realistic, but smoothed, bathymetry [Davey, 2004]. The model was forced by the Antarctic Mesoscale Prediction System, a mesoscale atmospheric forecast model [Bromwich *et al.*, 2005]. Rather than specifying surface fluxes due to sea ice from observations [Dinniman *et al.*, 2011], the version used here incorporated a coupled sea ice model [Budgell, 2005].

The model generates DSW over the continental shelf, primarily in polynyas along the Ross Ice Shelf front and close to the coast. The DSW then flows northward along the Drygalski and Glomar Challenger troughs (DT and GCT, respectively). These DSW flows are generally consistent with observations [Gordon *et al.*, 2009; Budillon *et al.*, 2011]. The DSW mixes with other water masses over the outer continental shelf and upper slope to form AABW. Most production of DSW occurs in winter, and northward advection of DSW also varies

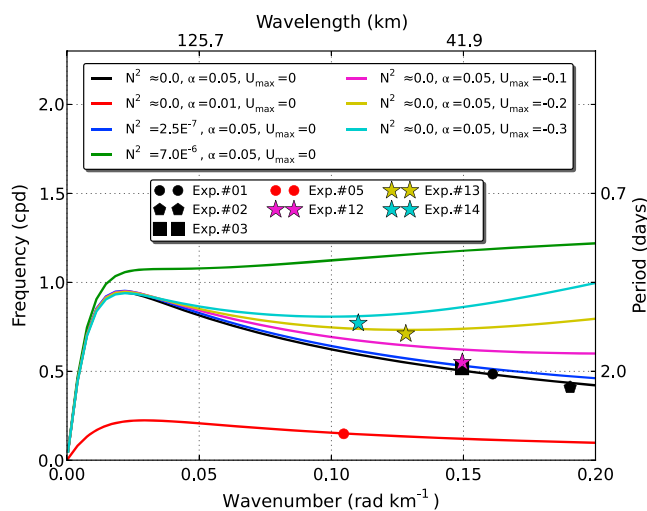


**Figure 2.** Dispersion curves from the *Brink* [2006] code (solid lines) using  $H_0 = 500$  m,  $|f| = 13.87 \times 10^{-5} \text{ s}^{-1}$  ( $72^\circ\text{S}$ ), for different ambient stratification ( $N^2$ ,  $\text{s}^{-2}$ ), slope ( $\alpha$ ), and westward along-slope flow ( $U_{\text{max}}$ ). Also shown are the frequency and wave number pairs calculated from time series of sea surface elevation extracted along the upper slope for selected model experiments. Color of each symbol matches color of the corresponding dispersion curve.

seasonally due to a strong annual cycle in the wind stress. Delivery of the densest DSW to the continental slope is delayed by several months relative to production farther south.

### 3. Results

#### 3.1. Idealized Simulations

The DSW prescribed at the southern boundary moves northward along the trough. Once it reaches the continental slope, most of the flow turns westward (left) due to the Earth’s rotation (since  $f < 0$ ), while a fraction descends to the abyss in a frictional bottom Ekman layer. In the control run (Experiment number 01), the velocity field to the east of the trough (Figure 1b) is wave-like, with a frequency ( $\omega$ ) of  $\sim 0.48$  cycles per day (cpd) and a wavelength ( $\lambda$ ) of  $\sim 39$  km (Table 1; Figure 2). Wave properties vary as functions of slope, total depth, and density anomaly. In all cases, frequencies (0.13–0.83 cpd) are subinertial ( $f(72^\circ) = 1.91$  cpd), wavelengths (29–66 km) are greater than  $R_d$ , and phase speeds  $c_p = \omega/k$  are westward (0.06–0.51  $\text{m s}^{-1}$ ). In experiments 01 to 13, energy propagates eastward (at the group speed  $c_g = \partial\omega/\partial k$ ), in the direction opposing both the dense outflow and  $c_p$  (Table 1). Westward energy propagation only occurs when westward  $U_{\text{max}}$  is large (Experiment number 14).

Good agreement between the frequencies and wavelengths and theoretical dispersion relations from *Brink* [2006] confirms that all 14 simulations generated TVWs (Figure 2). Eastward energy flux is possible only because the ambient stratification is very weak. The dispersion curves obtained using typical stratification for the Weddell and Ross seas ( $N^2 = 2.5 \times 10^{-7} \text{ s}^{-2}$ ) are very similar to the weak stratification case ( $N^2 \approx 0.0 \text{ s}^{-2}$ ) modeled here. Keeping other parameters consistent with our control run, but using a stratification value ( $N^2 = 7.0 \times 10^{-6} \text{ s}^{-2}$ ) taken from a typical oceanic profile near the Mediterranean outflow [*Price and Baringer, 1994*], changes the characteristics of the TVWs (compare black and green curves in Figure 2) so that energy flux is always westward. Similarly, in the presence of strong westward background mean flow, energy at the shortest wavelengths no longer propagates eastward. At particular wavelengths,  $c_g \approx 0$  (Experiment numbers 13 and 14).

The relationship between the normalized oscillation period ( $T/T_{\text{inertial}}$ ) and  $\Gamma_{\text{av}}$  (Figure 3) is consistent with results from laboratory experiments obtained by *Lane-Serff and Baines* [1998] and in an idealized numerical study by *Spall and Price* [1998, Figure 16b]. The physical mechanism behind the time dependence of these oscillations can be explained as follows. As the DSW exits the trough, it entrains the water above it. This ambient water is then stretched as it descends the slope and TVWs are excited as a consequence of potential vorticity conservation. The oscillation period decreases as the amount of stretching in the ambient water (with respect to  $D$ ) increases, with a limiting value of  $T \sim 2.3 \times T_{\text{inertial}}$  [*Lane-Serff and Baines, 1998*].

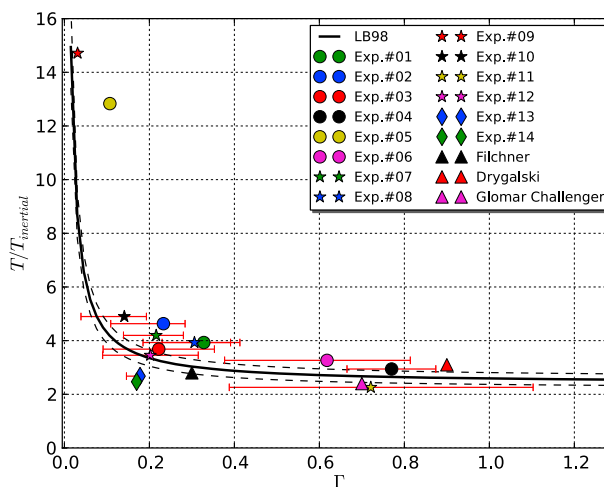


**Figure 3.** Wave period ( $T$ ) normalized by the domain-averaged inertial period ( $T_{inertial}$ ) as a function of the stretching parameter ( $\Gamma$ ) for all experiments listed in Table 1. The horizontal bars (red lines) are the 80% range of  $\Gamma(t)$  values for model time  $t = 70-100$  days (see also Table 1). The curves from Lane-Serff and Baines [1998] are plotted for comparison (solid line is the mean, and dashed lines show upper and lower limits). Also shown are representative values for the Filchner, Drygalski, and Glomar Challenger overflow plumes (see Table 2).

Two important parameters useful in defining the dynamical regime of overflows [Cenedese et al., 2004] are the Ekman number,  $Ek = (\delta/h_0)^2$ , where  $\delta$  is the Ekman layer thickness, and the Froude number,  $Fr = \Delta U / \sqrt{b_0 h_0}$ , where  $\Delta U$  is the velocity difference between the upper and bottom layers. Once the DSW exits the trough, all idealized simulations presented here are characterized by  $Fr > 1$  and  $0.1 < Ek < 1$  values which, according to the laboratory overflow experiments of Cenedese et al. [2004], justify the wave regime observed.

Typical values for the Filchner, Drygalski, and Glomar Challenger outflows yield  $\Gamma \approx 0.3, 0.9$ , and  $0.7$ , respectively (Table 2), the difference being primarily due to larger  $\alpha$  in the Ross Sea. When combined with the  $\sim 35$  h oscillation period associated with the TVWs that Jensen et al. [2013] observed next to the Filchner outflow, the 38 h oscillation found in a numerical study of the Drygalski outflow [Padman et al., 2009] and the  $\sim 30$  h observed in our realistic model (see the following section), these estimates show good agreement with the numerical results presented here (Figure 3). The data set analyzed by Jensen et al. [2013] showed seasonal variations in the evolution of the subinertial oscillations, with periods of  $\sim 39$  h during summer months and  $\sim 32$  h during winter months. Those authors showed that a stronger westward along-slope current during the winter months (which is the case for the Antarctic Slope Current) explains the higher frequencies observed during that season. Our results are consistent with their explanation, but we also show that wave frequency increases when the density anomaly of the outflow increases, increasing  $R_d$ .

### 3.2. Realistic Model of Ross Sea Outflows

Analyses of 1 year of output from our Ross Sea ROMS simulation (see section 2.2) show that oscillations with periods of  $\sim 30$  h occur along sections of the continental shelf north and east of the Drygalski and Glomar Challenger troughs (DT and GCT, respectively; see Figure 4e for locations). A Hovmöller diagram of the

**Table 2.** Estimated Stretching Parameter  $\Gamma$  and Shelf Waves Oscillation Period  $T$  for the Following Overflow Plumes: Filchner [Foldvik et al., 2004; Wang et al., 2009; Jensen et al., 2013], Drygalski [Padman et al., 2009; Muench et al., 2009], and Glomar Challenger (Section 3.2)

Variable	Filchner	Drygalski	Glomar Challenger
$R_d$ (km)	4	4.5	3
$\alpha$	0.03	0.1	0.1
$D$ (m)	400	500	400
$T_{inertial}$ (h)	12.47	12.65	12.65
$\Gamma$	0.3	0.9	0.7
$T/T_{inertial}$	2.8	3.2	2.4

band-passed (0.3–1 cpd), depth-averaged, cross-slope velocity (Figures 4a and 4b) shows westward phase propagation at  $c_p \approx 1.6 \text{ m s}^{-1}$  and eastward energy propagation with  $c_g \approx 0.5 \text{ m s}^{-1}$ , confirming that these oscillations are the short-wavelength mode of the TVW dispersion curves. The TVWs propagate several hundred kilometers eastward from their sources.

The realistic, time-varying atmospheric forcing in this simulation modulates DSW production,  $U_{max}$  and ambient stratification, causing temporal changes in production and propagation of TVWs.

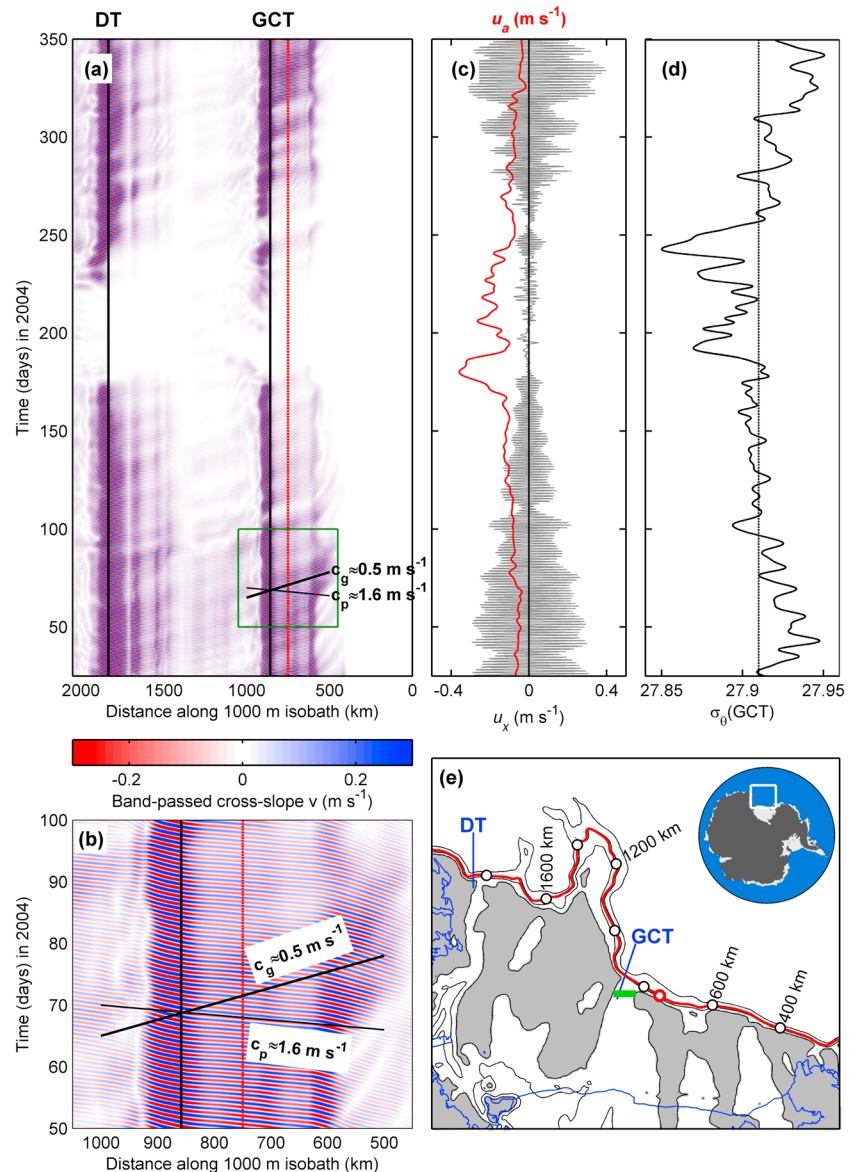


**Figure 4.** (a) Hovmöller diagram for band-passed (0.3–1 cycle per day (cpd)) cross-slope, depth-averaged velocity as a function of time in days of 2004 (y axis) and distance (x axis) along the 1000 m isobath (red contour in Figure 4e), representing the upper continental slope in the Ross Sea, Antarctica. Black vertical lines indicate western edges of the Drygalski Trough (DT) and Glomar Challenger Trough (GCT); see Figure 4e for locations. Red line is location of a point ~100 km east of GCT; see red circle on 1000 m isobath in Figure 4e. Typical values of group velocity ( $c_g$ ) and phase velocity ( $c_p$ ) are indicated. (b) Expanded view for the region indicated by the green box in Figure 4a, to clarify phase propagation. The color scale for both Figures 4a and 4b is provided between these two panels. (c) Band-passed (0.3–1 cpd), across-slope (gray), and low-passed (<0.3 cpd) along-slope (red) velocity components at the 1000 m isobath, at the point ~100 km west of GCT. (d) Mean potential density averaged along a transect across the northern GCT, for all model coordinate depths below 300 m; see green line in Figure 4e for location. Vertical line at  $\sigma_\theta = 27.91$  is the approximate value below which TVWs are not found. (e) Map of Ross Sea. Shaded areas are water depths shallower than 530 m; black contours show 750 and 1500 m isobaths. Red line shows 1000 m isobath. Open circles are every 200 km along the isobath.

For example, at a location ~100 km east of the GCT, cross-slope velocity associated with the TVWs can vary from negligible to  $>0.25 \text{ m s}^{-1}$  (Figure 4c) through the year, with some modulation also on shorter time scales. This modulation provides the signal of eastward energy propagation seen in Figure 4a.

The variability in TVW energy is correlated with seasonal changes in the strength of the along-slope mean flow (Figure 4b) and mean potential density ( $\sigma_\theta$ ) of the deep water in the northern GCT (Figure 4d). The loss

of TVWs in winter (days 180–260) corresponds with stronger westward flows and low  $\sigma_\theta$  in the GCT, consistent with the results from our set of idealized models.

#### 4. Summary

Our idealized simulations demonstrate that outflows of dense shelf water (DSW) from the Antarctic shelf seas onto the continental slope generate topographic vorticity waves (TVWs) that then propagate along the slope. The properties of these waves are consistent with observed variability along the southern Weddell Sea continental slope near the Filchner Trough outflow. The period ( $T$ ) of the TVWs decreases as the stretching parameter  $\Gamma$  increases, implying that higher frequency waves will be generated when the continental slope is steeper and when the density anomaly of the outflow is increased. In addition, stronger mean westward along-slope flows, representing the Antarctic Slope Current, will reduce the wave period. For most of our model configurations, the energy flux of the TVWs is eastward from the trough, opposing the westward transport of the dense outflow and the TVWs' phase propagation. Westward TVW energy flux only occurs when the mean westward along-slope flow is sufficiently strong.

In our idealized simulations and in our realistic model of the Ross Sea, the TVW cross-slope currents often exceed  $0.2 \text{ m s}^{-1}$ , suggesting that they contribute to mixing and cross-slope advection in the vicinity of troughs. These are regions of important cross-slope exchanges—outflows of DSW leading to AABW production and inflows of heat onto the continental shelf and south to the ice shelves—implying that our ability to represent these exchanges depends on accurate models of TVW production, propagation, and dissipation (not discussed here). The realistic Ross Sea model demonstrates strong time dependence of TVW energy east of Drygalski and Glomar Challenger troughs, correlated with seasonal variability of DSW properties and along-slope mean flow.

We conclude that TVWs generated by DSW outflows from Antarctic shelf seas play a role in processes linking the circulation of the deep Southern Ocean to continental shelf processes including southward heat advection, sea ice and DSW formation, and ice shelf mass loss through basal melting. Furthermore, since cross-slope advection and mixing by TVWs contributes to the background state in which the TVWs are generated and propagate, the effect of these waves cannot be simply parameterized as an added source of kinetic energy. Instead, we expect feedback between the TVWs and the background state, requiring explicit representation of these processes in models representing the role of Antarctic shelf seas in the global climate system.

#### Acknowledgments

This study was funded by the National Science Foundation, grants OCE-0961405 and OCE-0722644 (MRI) to Earth & Space Research (ESR) and OCE-0961369 to the University of Miami. We thank K. Brink (WHOI) for providing the code for calculating dispersion curves for inviscid coastal-trapped waves and M. Dinniman (Old Dominion University) for developing the realistic ROMS model of the Ross Sea. We also thank University of Miami's Center for Computational Science for making available their resources. We thank two anonymous reviewers for their constructive comments on this paper. This is ESR contribution 149.

The Editor thanks two anonymous reviewers for their assistance in evaluating this paper.

#### References

- Brink, K. H. (2006), Coastal-trapped waves with finite bottom friction, *Dyn. Atmos. Oceans*, 41(3), 172–190.
- Bromwich, D. H., A. J. Monaghan, K. W. Manning, and J. G. Powers (2005), Real-time forecasting for the Antarctic: An evaluation of the Antarctic Mesoscale Prediction System (AMPS)\*, *Mon. Weather Rev.*, 133(3), 579–603.
- Budgell, W. (2005), Numerical simulation of ice-ocean variability in the barents sea region, *Ocean Dyn.*, 55(3–4), 370–387.
- Budillon, G., P. Castagno, S. Aliani, G. Spezie, and L. Padman (2011), Thermohaline variability and Antarctic bottom water formation at the Ross Sea shelf break, *Deep Sea Res. Part I*, 58(10), 1002–1018, doi:10.1016/j.dsr.2011.07.002.
- Cenedese, C., J. A. Whitehead, T. Ascarelli, and M. Ohiwa (2004), A dense current flowing down a sloping bottom in a rotating fluid, *J. Phys. Oceanogr.*, 34(1), 188–203.
- Davey, F. (2004), *Ross Sea Bathymetry, 1:2,000,000, Version 1.0, Institute of Geological & Nuclear Sciences Geophysical Map 16*, Institute of Geological & Nuclear Sciences Limited, Lower Hutt, New Zealand.
- Dinniman, M. S., J. M. Klinck, and W. O. Smith (2011), A model study of Circumpolar Deep Water on the West Antarctic Peninsula and Ross Sea continental shelves, *Deep Sea Res. Part II*, 58(13–16), 1508–1523, doi:10.1016/j.dsr2.2010.11.013.
- Foldvik, A., T. Gammelsrød, S. Østerhus, E. Fahrbach, G. Rohardt, M. Schröder, K. W. Nicholls, L. Padman, and R. A. Woodgate (2004), Ice shelf water overflow and bottom water formation in the southern Weddell Sea, *J. Geophys. Res.*, 109, C02015, doi:10.1029/2003JC002008.
- Gill, A. (1973), Circulation and bottom water production in the Weddell Sea, *Deep Sea Res.*, 20, 111–140.
- Gordon, A. L., A. H. Orsi, R. Muench, B. A. Huber, E. Zambianchi, and M. Visbeck (2009), Western Ross Sea continental slope gravity currents, *Deep Sea Res. Part II*, 56(13–14), 796–817, doi:10.1016/j.dsr2.2008.10.037.
- Heywood, K. J., R. A. Locarnini, R. D. Frew, P. F. Dennis, and B. A. King (1998), Transport and water masses of the Antarctic Slope Front system in the eastern Weddell Sea, in *Ocean, Ice, and Atmosphere: Interactions at the Antarctic Continental Margin*, vol. 75, edited by S. S. Jacobs and R. F. Weiss, pp. 203–214, Antarctic Research Series, AGU, Washington D. C.
- Ilicak, M., T. Özgökmen, H. Peters, H. Baumert, and M. Iskandarani (2008), Performance of two-equation turbulence closures in three-dimensional simulations of the Red Sea overflow, *Ocean Modell.*, 24(3–4), 122–139, doi:10.1016/j.ocemod.2008.06.001.
- Ilicak, M., S. Legg, A. Adcroft, and R. Hallberg (2011), Dynamics of a dense gravity current flowing over a corrugation, *Ocean Modell.*, 38(1–2), 71–84, doi:10.1016/j.ocemod.2011.02.004.
- Jacobs, S. S. (1991), On the nature and significance of the Antarctic Slope Front, *Mar. Chem.*, 35(1), 9–24.
- Jensen, M. F., I. Fer, and E. Darelius (2013), Low frequency variability on the continental slope of the southern Weddell Sea, *J. Geophys. Res. Oceans*, 118, 4256–4272, doi:10.1002/jgrc.20309.

- Lane-Serff, G., and P. Baines (1998), Eddy formation by dense flows on slopes in a rotating fluid, *J. Fluid Mech.*, *363*, 229–252.
- Legg, S., R. Hallberg, and J. Girton (2006), Comparison of entrainment in overflows simulated by z-coordinate, isopycnal and non-hydrostatic models, *Ocean Modell.*, *11*(1–2), 69–97, doi:10.1016/j.ocemod.2004.11.006.
- Muench, R., L. Padman, A. Gordon, and A. Orsi (2009), A dense water outflow from the Ross Sea, Antarctica: Mixing and the contribution of tides, *J. Mar. Syst.*, *77*(4), 369–387, doi:10.1016/j.jmarsys.2008.11.003.
- Orsi, A. (1999), Circulation, mixing, and production of Antarctic Bottom Water, *Prog. Oceanogr.*, *43*(1), 55–109, doi:10.1016/S0079-6611(99)00004-X.
- Padman, L., S. L. Howard, A. H. Orsi, and R. D. Muench (2009), Tides of the northwestern Ross Sea and their impact on dense outflows of Antarctic Bottom Water, *Deep Sea Res. Part I*, *56*(13–14), 818–834, doi:10.1016/j.dsr2.2008.10.026.
- Platzman, G., G. Curtis, K. S. Hansen, and R. D. Slater (1981), Normal modes of the World Ocean. Part II: Description of modes in the period range 8 to 80 hours, *J. Phys. Oceanogr.*, *11*, 579–603.
- Price, J., and M. Baringer (1994), Outflows and deep water production by marginal seas, *Prog. Oceanogr.*, *33*, 161–200.
- Shchepetkin, A. F., and J. C. McWilliams (2005), The Regional Oceanic Modeling System (ROMS): A split-explicit, free-surface, topography-following-coordinate oceanic model, *Ocean Modell.*, *9*(4), 347–404, doi:10.1016/j.ocemod.2004.08.002.
- Spall, M., and J. Price (1998), Mesoscale variability in Denmark strait: The PV outflow hypothesis\*, *J. Phys. Oceanogr.*, *28*, 1598–1623.
- Wang, Q., S. Danilov, and J. Schröter (2009), Bottom water formation in the southern Weddell Sea and the influence of submarine ridges: Idealized numerical simulations, *Ocean Modell.*, *28*(1–3), 50–59, doi:10.1016/j.ocemod.2008.08.003.